ELEKTRİK, VOL.6, NO.2, 1998, ©TÜBİTAK EMO

# Adaptive Shape From Shading

**Atilla Gültekin & Muhittin Gökmen**
*Department of Computer Science,*
*Electrical and Electronics Faculty*
*İstanbul Technical University,*
*80626 Maslak, İstanbul - TURKEY*
*e-mail: 100631.335@compuserve.com*
*gokmen@cs.itu.edu.tr*

**Abstract**

*Extracting surface orientation and surface depth from one or more images is one of the classic problems in computer vision. Shape-from-shading (SFS) deals with the recovery of 3-D shape from a single shaded image. The shape is recovered by minimizing an energy functional involving constraints such as smoothness. In this constrained problem, although the smoothness constraint helps to stabilize the minimization process, it pushes the reconstruction toward a smooth surface. In this paper, we present a new adaptive shape-from-shading method which reduces this oversmoothing by controlling the smoothness spatially over the image space. In order to improve the quality of the reconstruction, we also integrated this adaptive SFS algorithm and photometric stereo technique to recover shape by using more than one input image. The new algorithm is robust, data driven and updates both the gradient field and height map simultaneously. A hierarchical implementation of the algorithm is presented. Typical SFS and photometric stereo results are given to illustrate the usefulness of our approach.*
*Index Terms – Computer vision, regularization, surface reconstruction, shape from shading*

## 1. Introduction

Shape-from-shading (SFS) [1] is one of the classic research problems in computer vision. SFS deals with the recovery of surface orientation and surface shape (height) from the gradual variation of shading in the image. SFS is implemented by first modeling the image brightness as a function of surface geometry and then reconstructing a surface which, under the given imaging model, generates an image close to the input image. This field was formally introduced by Horn [2, 3] and there have been many significant improvements in both theoretical and practical aspects of the problem.

Shape-from-photometric-stereo [4] is another method for shape recovery in computer vision. The difference between shape-from-photometric-stereo and SFS is in the number of input images. Shape-from-photometric-stereo recovers shape from *multiple* intensity images of the same scene generated using fixed viewing direction and different light source directions; while SFS provides the shape estimate from a *single* image. Thus, using multiple images which are taken with different lighting provides additional information for robust surface reconstruction.

Since a single measurement of image brightness provides only limited information about surface orientation, additional constraints such as smoothness must be used in order to find a unique solution.

Although this smoothness term is used to ensure the convergence of the iterative process, it flattens the SFS reconstruction. The solution of this problem is to use an adaptive smoothing function to reduce oversmoothing along the reconstructed image. In this paper, we introduce a new SFS approach in which the smoothness is controlled spatially over the image space [5]. The adaptive nature of the algorithm eliminates the selection of the optimum value of smoothness parameter and protects the solution "to walk away" from the ground truth, even if the ground truth is used as an initial condition [6]. Using calculus of variations [7] and a linear approximation of the reflectance map [6], a new iterative scheme which simultaneously updates the slope and height is developed. A hierarchical implementation of the SFS algorithm is also presented.

## 2. Formulation

In the usual formulation, the surface reflectance map $R(p,q)$ is known, so that the shaded image provides a single constraint on the surface gradient $(p,q)$ at each point in the image. Additional constraints, such as requiring that the gradient vary smoothly and that the gradient field be integrable, are then used to find a unique solution for the surface.

Different parts of the surface are oriented differently and thus will appear with different brightness. This spatial variation of brightness, or *shading*, is used to estimate the orientation of surface patches. For a surface of uniform reflectivity, where the light source and the viewer are sufficiently distant and there is no inter-reflection between objects, shading can be captured in the *reflectance map* $R(p,q)$, where $p$ and $q$ are surface gradient components

$$p = \frac{\partial z}{\partial x} \qquad \text{and} \qquad q = \frac{\partial z}{\partial y}, \tag{1}$$

$z(x,y)$ is the height field, and the $z$ axis points towards the viewer. The above description tells us how a shaded image is determined by the local orientation of the surface. In SFS, however, we must solve the inverse problem; i.e., given a shaded image, we must find the surface which generated it. The reflectance map together with the shaded image gives us one constraint on the solution. In the following, we describe this constraint with three others used in SFS problems.

### 2.1. Brightness Constraint

The brightness constraint is based on the image irradiance equation

$$I(x,y) = \beta R(p,q) \tag{2}$$

where $I(x,y)$ is the intensity observed at the point $(x,y)$ in the image and $R(p,q)$ is the reflectance map applied to the surface gradient $(p,q)$ at that point. The proportionality constant $\beta$ can be set to 1 by rescaling the intensity image or chosen so that the maximum possible brightness is $I = 1$. For the Lambertian surface, we write

$$R(p,q) = \cos\theta_i = \eta\,\frac{\cos\sigma - p\sin\sigma\cos\tau - q\sin\sigma\sin\tau}{\sqrt{1+p^2+q^2}} \tag{3}$$

where $\theta_i$ is the incident angle between the surface normal and the light source direction, $\eta$ is the albedo, $\sigma$ and $\tau$ are the slant and the tilt angles of the illuminant, respectively.

To use the image irradiance equation as a brightness constraint, we measure the total squared brightness error over the image

$$F_1(p,q) = \iint (I(x,y) - R(p,q))^2\,dx\,dy. \tag{4}$$

This cost functional is then used as a part of an energy functional which is minimized with respect to $(p, q)$ to find the solution of the shape-from-shading problem.

### 2.2. Smoothness Constraint

To help stabilize the iterative shape-from-shading algorithm and to ensure that it has a unique minimum, we use

$$F_2(p,q) = \iint (p_x^2 + p_y^2 + q_x^2 + q_y^2)\, dx\, dy \tag{5}$$

where $p_x$, $p_y$, $q_x$ and $q_y$ are the partial derivatives of the surface gradient.

### 2.3. Integrability Constraint

To ensure that the gradient field $(p, q)$ computed by the shape-from-shading algorithm corresponds to a valid surface we use

$$F_3(p,q,z) = \iint ((z_x - p)^2 + (z_y - q)^2)\, dx\, dy \tag{6}$$

where $z_x$ and $z_y$ are the partial derivatives of the height field $z$.

### 2.4. Intensity Gradient Constraint

To require that the gradients of the reconstructed image be close to the gradients of the input image in both $x$ and $y$ directions, we use

$$F_4(p,q) = \iint ((R_x - I_x)^2 + (R_y - I_y)^2)\, dx\, dy. \tag{7}$$

### 2.5. Coupled Height and Gradient Estimation using Integrated Constraints

The constraints presented above have been used in various combinations in the previous SFS algorithms. In our implementation, we combine all four SFS constraints in a single functional to obtain a general purpose algorithm and use a spatially controlled regularization parameter instead of a fixed regularization parameter in order to adaptively control the smoothness over the image space. To achieve this, we construct the following energy functional

$$F(p,q,z) = F_1(p,q) + F_2^{'}(p,q) + \mu\, F_3(p,q,z) + \beta\, F_4(p,q) \tag{8}$$

where $F_1$ is the brightness constraint,

$$F_2^{'}(p,q) = \iint \lambda(x,y)\, (p_x^2 + p_y^2 + q_x^2 + q_y^2)\, dx\, dy \tag{9}$$

is the spatially controlled constraint, $F_3$ is the integrability constraint and $F_4$ is the intensity gradient constraint. In this energy functional, $\lambda(x, y)$ is a function of spatial coordinates while $\mu$ and $\beta$ are the scalars. Minimizing (8) or equivalently solving associated Euler equations produces both a gradient field $(p, q)$ and a surface $z(x, y)$ which best fits this gradient.

In our iterative process, the space varying regularization parameter at location $(x, y)$ is determined by the following function:

$$\lambda_{new}(x,y) = \begin{cases} \mathcal{F}(x,y,\lambda_{old}) & \text{if } c(x,y) > 0 \text{ and } \lambda_{old} > \lambda_{min} \\ \lambda_{old}(x,y) & otherwise \end{cases} \tag{10}$$

where

$$\mathcal{F}(x,y,\lambda_{old}) = (1 - e^{-\frac{c(x,y)}{V_T}})\,\lambda_{min} + (e^{-\frac{c(x,y)}{V_T}})\,\lambda_{old}(x,y), \tag{11}$$

$c(x,y)$ is the control signal, $V_T$ is a time-constant that controls the rate of exponential decrease and $\lambda_{min}$ is a preselected minimum value that $\lambda(x,y)$ may have. The control signal is defined as $c(x,y) = abs(I(x,y) - R(p,q))$, where $abs()$ denotes the absolute value and the function $\mathcal{F}(x,y,\lambda_{old})$ is an exponentially decreasing function with the following properties:

$$\lim_{c(x,y)\to 0} \mathcal{F}(x,y,\lambda_{old}) = \lambda_{old}(x,y) \quad \text{and} \quad \lim_{c(x,y)\to\infty} \mathcal{F}(x,y,\lambda_{old}) = \lambda_{min}, \tag{12}$$

so that the regularization parameter is only allowed to decrease during iterations.

Using the calculus of variations, minimizing (8) is equivalent to solving the following Euler equations:

$$\begin{aligned} F_p - \frac{\partial}{\partial x}F_{p_x} - \frac{\partial}{\partial y}F_{p_y} &= 0 \\ F_q - \frac{\partial}{\partial x}F_{q_x} - \frac{\partial}{\partial y}F_{q_y} &= 0 \\ F_z - \frac{\partial}{\partial x}F_{z_x} - \frac{\partial}{\partial y}F_{z_y} &= 0 \end{aligned} \tag{13}$$

where subscripts denote the partial derivatives.

Approximating the reflectance map in (8) around $(p,q)$ by Taylor series expansion of up to first-order terms and replacing in (13), we obtain

$$\begin{pmatrix} A_{11} & A_{12} & 0 \\ A_{21} & A_{22} & 0 \\ 1 & 1 & -4 \end{pmatrix} \begin{pmatrix} \delta p \\ \delta q \\ \delta z \end{pmatrix} = \begin{pmatrix} B_1 + \frac{1}{4}\mu B_3 \\ B_2 + \frac{1}{4}\mu B_3 \\ B_3 \end{pmatrix} \tag{14}$$

where

$$\begin{aligned} A_{11} &= 4\lambda + \lambda_x + \lambda_y + \frac{5}{4}\mu + R_p^2(1+4\beta) \\ A_{12} &= A_{21} = \frac{1}{4}\mu + R_p R_q(1+4\beta) \\ A_{22} &= 4\lambda + \lambda_x + \lambda_y + \frac{5}{4}\mu + R_q^2(1+4\beta) \\ B_1 &= \lambda(p_{xx} + p_{yy}) + \lambda_x p_x + \lambda_y p_y + \mu(z_x - p) \\ &\quad + R_p\{I - R + \beta[(p_{xx} + p_{yy})R_p + (q_{xx} + q_{yy})R_q - I_{xx} - I_{yy}]\} \\ B_2 &= \lambda(q_{xx} + q_{yy}) + \lambda_x q_x + \lambda_y q_y + \mu(z_y - q) \\ &\quad + R_q\{I - R + \beta[(p_{xx} + p_{yy})R_p + (q_{xx} + q_{yy})R_q - I_{xx} - I_{yy}]\} \\ B_3 &= p_x + q_y - z_{xx} - z_{yy}. \end{aligned}$$

and $(\delta p, \delta q, \delta z)$ are the increments in $(p,q,z)$ after an iteration. Solving (14) for $(\delta p, \delta q, \delta z)$, we obtain the updating scheme

$$\begin{aligned} \delta p &= \frac{1}{\Delta}[A_{22}(B_1 + \frac{1}{4}\mu B_3) - A_{12}(B_2 + \frac{1}{4}\mu B_3)] \\ \delta q &= \frac{1}{\Delta}[A_{11}(B_2 + \frac{1}{4}\mu B_3) - A_{12}(B_1 + \frac{1}{4}\mu B_3)] \end{aligned} \tag{15}$$

$$\delta z = \frac{1}{4}(\delta p + \delta q - B_3) \tag{16}$$

where $\Delta = A_{11}A_{22} - A_{12}^2$.

## 3. Hierarchical Structure

The solution to the shape-from-shading problem requires long-range error to be reduced through strictly local interactions. This situation arises mainly from the local nature of the representation used for gradient and height fields and causes very large number of iterations in the iterative scheme. Multigrid methods are often used in computer vision to speed up computationally intensive tasks such as shape-from-shading. In these methods, an approximate solution computed for a reduced image is used to guide the algorithm toward the complete solution on a larger image.

Multigrid implementation can be simplified by having a $2:1$ decrease in grid nodes during a transition from a finer grid to an adjacent coarser grid. Thus, the image resolution is reduced by a factor of 2 between adjacent resolution layers. We use the simplest pyramid method for image sampling and interpolation. The grid size for the lowest layer is $32\text{x}32$. The input images for various resolution layers are derived from the given highest resolution image by averaging the pixels that belong to the same cell in the low-resolution layer. Let the variables with a tilde ($\tilde{}$) stand for the shape descriptors of the higher resolution layer while the variables without tilde denote those of the lower resolution layer. Then, the communication of the results from one layer to another are specified by the following rules:

*Rule 1:* The illuminant direction and albedo are the same

$$(\tilde{\sigma}, \tilde{\tau}, \tilde{\eta}) = (\sigma, \tau, \eta).$$

This assumption is made based on experiments reported in [8] that the estimated illuminant direction and surface albedo almost insensitive to changes in resolution. However, the illuminant direction and albedo can also be estimated for each layer independently.

*Rule 2:* The surface descriptions of a higher resolution layer are interpolated from the descriptions of the adjacent lower resolution layer. Let $\tilde{N}$ be the image size of the higher resolution layer. For $i, j \in \{2, \ldots, \tilde{N}\}$, the shape descriptions for the higher resolution layer are

$$(\tilde{p}, \tilde{q}, \tilde{z})_{i,j} = \begin{cases} (p, q, 2z)_{\frac{i}{2}, \frac{j}{2}}, & \text{if } i \text{ and } j \text{ are evens} \\ \frac{1}{2}[(p, q, 2z)_{\frac{i+1}{2}, \frac{j}{2}} + (p, q, 2z)_{\frac{i-1}{2}, \frac{j}{2}}], & \text{if } i \text{ is odd and } j \text{ is even} \\ \frac{1}{2}[(p, q, 2z)_{\frac{i}{2}, \frac{j+1}{2}} + (p, q, 2z)_{\frac{i}{2}, \frac{j-1}{2}}], & \text{if } i \text{ is even and } j \text{ is odd} \\ \frac{1}{4}[(p, q, 2z)_{\frac{i+1}{2}, \frac{j+1}{2}} + (p, q, 2z)_{\frac{i+1}{2}, \frac{j-1}{2}} & \\ +(p, q, 2z)_{\frac{i-1}{2}, \frac{j+1}{2}} + (p, q, 2z)_{\frac{i-1}{2}, \frac{j-1}{2}}] & \text{if } i \text{ and } j \text{ are odds.} \end{cases}$$

*Rule 3:* The natural boundary condition is used for the interpolation of boundary pixels. For example, for the boundaries of $i = 1$ and $j = 1$,

$$\begin{array}{lll} (\tilde{p}, \tilde{q})_{1,j} = 2(\tilde{p}, \tilde{q})_{2,j} - (\tilde{p}, \tilde{q})_{3,j} & \tilde{z}_{1,j} = \tilde{z}_{2,j} - \tilde{p}_{1,j}, & \text{for } j \geq 2 \\ (\tilde{p}, \tilde{q})_{i,1} = 2(\tilde{p}, \tilde{q})_{i,2} - (\tilde{p}, \tilde{q})_{i,3} & \tilde{z}_{i,1} = \tilde{z}_{i,2} - \tilde{q}_{i,1}, & \text{for } i \geq 2 \\ (\tilde{p}, \tilde{q})_{1,1} = 2(\tilde{p}, \tilde{q})_{2,2} - (\tilde{p}, \tilde{q})_{3,3} & \tilde{z}_{1,1} = \tilde{z}_{2,2} - \tilde{p}_{1,1} + \tilde{q}_{1,1}. & \end{array}$$

## 4. Iterative Scheme

Combining the hierarchical implementation and our new adaptive approach, we obtain the following robust shape-from-shading scheme:

1. Estimate the reflectance map parameters $(\sigma, \tau, \eta)$.

2. Normalize the input image: $\bar{I}(x,y) = I(x,y) \,/\, \eta$.

3. Reduce the input image size to that of the lowest resolution layer.

4. a) Input the initial status $p^0$, $q^0$ and $z^0$.
   b) Initially set the regularization parameters at each pixel to the maximum value, i.e., $\lambda(x,y) = \lambda_{max}$ and set $\lambda_{min}$.
   c) Set the values for $\mu$ and $\beta$.

5. Update the current surface shape. For each pixel, the partial derivatives are approximated by using the forward finite differences. The reconstructed shape is updated by

$$\begin{aligned} p^{k+1} &= p^k + \delta p \\ q^{k+1} &= q^k + \delta q \\ z^{k+1} &= z^k + \delta z \end{aligned}$$

and

$$\begin{aligned} \delta p &= \frac{1}{\Delta}[A_{22}(B_1 + \frac{1}{4}\mu B_3) - A_{12}(B_2 + \frac{1}{4}\mu B_3)] \\ \delta q &= \frac{1}{\Delta}[A_{11}(B_2 + \frac{1}{4}\mu B_3) - A_{12}(B_1 + \frac{1}{4}\mu B_3)] \\ \delta z &= \frac{1}{4}(\delta p + \delta q - B_3) \end{aligned}$$

where

$$\begin{aligned} A_{11} &= 4\lambda + \lambda_x + \lambda_y + \frac{5}{4}\mu + R_p^2(1+4\beta) \\ A_{12} &= \frac{1}{4}\mu + R_p R_q(1+4\beta) \\ A_{22} &= 4\lambda + \lambda_x + \lambda_y + \frac{5}{4}\mu + R_q^2(1+4\beta) \\ B_1 &= \lambda(p_{xx} + p_{yy}) + \lambda_x p_x + \lambda_y p_y + \mu(z_x - p) \\ &\quad + R_p\{I - R + \beta[(p_{xx} + p_{yy})R_p + (q_{xx} + q_{yy})R_q - I_{xx} - I_{yy}]\} \\ B_2 &= \lambda(q_{xx} + q_{yy}) + \lambda_x q_x + \lambda_y q_y + \mu(z_y - q) \\ &\quad + R_q\{I - R + \beta[(p_{xx} + p_{yy})R_p + (q_{xx} + q_{yy})R_q - I_{xx} - I_{yy}]\} \\ B_3 &= p_x + q_y - z_{xx} - z_{yy} \\ R_p &= [R(p^k_{(x,y)} + \delta, q^k_{(x,y)}) - R(p^k_{(x,y)}, q^k_{(x,y)})] \,/\, \delta \\ R_q &= [R(p^k_{(x,y)}, q^k_{(x,y)} + \delta) - R(p^k_{(x,y)}, q^k_{(x,y)})] \,/\, \delta \\ \Delta &= A_{11}A_{22} - A_{12}^2. \end{aligned}$$

6. Go to the next step if solution is stable or iterations has reached $N_{max}$ of current layer; otherwise repeat Step 5.

7. Compute the control signal $c(x,y) = abs(I(x,y) - R(p^k_{(x,y)}, q^k_{(x,y)}))$.

8. Update $\lambda(x,y)$ according to the following rule:

$$\lambda_{new}(x,y) = \begin{cases} \mathcal{F}(x,y,\lambda_{old}) & \text{if } c(x,y) > 0 \text{ and } \lambda_{old} > \lambda_{min} \\ \lambda_{old}(x,y) & otherwise \end{cases} \tag{17}$$

where

$$\mathcal{F}(x, y, \lambda_{old}) = (1 - e^{-\frac{c(x,y)}{V_T}})\,\lambda_{min} + (e^{-\frac{c(x,y)}{V_T}})\,\lambda_{old}(x, y).$$

9. If no change in $\lambda(x, y)$ values continue to Step 10; otherwise go back to Step 5 and repeat the process with new $\lambda(x, y)$ values.

10. If current image is in the highest resolution stop; otherwise
    a) Increase the image size and expand the shape reconstruction to the adjacent higher resolution layer,
    b) Expand $\lambda(x, y)$,
    c) Reduce the normalized input image to the current resolution,
    d) go to Step 5.

## 5. Relationship to Existing Techniques

In our adaptive shape-from-shading implementation, we combined all SFS constraints in a single energy functional. Thus, we have a general purpose algorithm which encompasses most of the existing methods. These methods are special instances of this generalized method and can be obtained by appropriately selecting parameter values.

In our method, we made $\lambda$ as a function of spatial coordinates, i.e., $\lambda(x, y)$, in order to control the degree of smoothness of the reconstructed surface. If we set a constant value to $\lambda$ and drop the intensity gradient constraint in the integrand $(\beta = 0)$, we obtain the scheme developed by Horn [6]. If we make $\lambda$ constant and drop both the integrability and the intensity gradient constraints ($\mu = 0$ and $\beta = 0$), we derive the algorithm presented by Ikeuchi and Horn [9]. If we instead remove both the departure from smoothness and the intensity gradient terms ($\lambda = 0$ and $\beta = 0$), we obtained something reminiscent of the iterative scheme of Strat [1], although Strat dealt with the integrability in a different way. We find Zheng and Chellappa's scheme [10] if we drop the departure from smoothness term $(\lambda = 0)$ in our method.

## 6. Integrating Photometric Stereo and Adaptive SFS

To recover surface orientation locally, we must introduce additional information. To determine two unknowns, $p$ and $q$, we need two equations. Two images, taken with different lighting, will yield two equations for each image point:

$$I = R(p, q) \qquad \text{and} \qquad \hat{I} = \hat{R}(p, q). \tag{18}$$

We also applied our adaptive regularization approach to the photometric stereo technique in order to improve the quality of the reconstructed surface obtained by the iterative scheme.

Suppose we have two input images, $I(x, y)$ and $\hat{I}(x, y)$, illuminated by two light sources placed different locations in the image space as $(\sigma, \tau)$ and $(\hat{\sigma}, \hat{\tau})$ respectively. Let the reflectance maps corresponding to these illuminant directions be

$$R(p, q) \;=\; \eta\, \frac{\cos\sigma - p\sin\sigma\cos\tau - q\sin\sigma\sin\tau}{\sqrt{1 + p^2 + q^2}} \tag{19}$$

$$\hat{R}(p, q) \;=\; \hat{\eta}\, \frac{\cos\hat{\sigma} - p\sin\hat{\sigma}\cos\hat{\tau} - q\sin\hat{\sigma}\sin\hat{\tau}}{\sqrt{1 + p^2 + q^2}}. \tag{20}$$

Then, for the photometric stereo, we use the functional

$$F(p,q,z) = F_1^{'}(p,q) + F_2^{'}(p,q) + \mu\, F_3(p,q,z) + \beta\, F_4(p,q) \tag{21}$$

where

$$F_1^{'}(p,q) = \int\!\!\int \{(I(x,y) - R(p,q))^2 + (\hat{I}(x,y) - \hat{R}(p,q))^2\}\, dx\, dy \tag{22}$$

and other terms, $F_2^{'}$, $F_3$ and $F_4$ are the same as terms given in Section 2.

From the Euler equations (13), we have

$$\begin{pmatrix} A_{11} & A_{12} & 0 \\ A_{21} & A_{22} & 0 \\ 1 & 1 & -4 \end{pmatrix} \begin{pmatrix} \delta p \\ \delta q \\ \delta z \end{pmatrix} = \begin{pmatrix} B_1 + \frac{1}{4}\mu B_3 \\ B_2 + \frac{1}{4}\mu B_3 \\ B_3 \end{pmatrix} \tag{23}$$

where

$$\begin{aligned}
A_{11} &= 4\lambda + \lambda_x + \lambda_y + \frac{5}{4}\mu + (R_p^2 + \hat{R}_p^2)(1+4\beta) \\
A_{12} &= A_{21} = \frac{1}{4}\mu + (R_p R_q + \hat{R}_p \hat{R}_q)(1+4\beta) \\
A_{22} &= 4\lambda + \lambda_x + \lambda_y + \frac{5}{4}\mu + (R_q^2 + \hat{R}_q^2)(1+4\beta) \\
B_1 &= \lambda(p_{xx} + p_{yy}) + \lambda_x p_x + \lambda_y p_y + \mu(z_x - p) \\
&\quad + R_p\{I - R + \beta[(p_{xx} + p_{yy})R_p + (q_{xx} + q_{yy})R_q - I_{xx} - I_{yy}]\} \\
&\quad + \hat{R}_p\{\hat{I} - \hat{R} + \beta[(p_{xx} + p_{yy})\hat{R}_p + (q_{xx} + q_{yy})\hat{R}_q - \hat{I}_{xx} - \hat{I}_{yy}]\} \\
B_2 &= \lambda(q_{xx} + q_{yy}) + \lambda_x q_x + \lambda_y q_y + \mu(z_y - q) \\
&\quad + R_q\{I - R + \beta[(p_{xx} + p_{yy})R_p + (q_{xx} + q_{yy})R_q - I_{xx} - I_{yy}]\} \\
&\quad + \hat{R}_q\{\hat{I} - \hat{R} + \beta[(p_{xx} + p_{yy})\hat{R}_p + (q_{xx} + q_{yy})\hat{R}_q - \hat{I}_{xx} - \hat{I}_{yy}]\} \\
B_3 &= p_x + q_y - z_{xx} - z_{yy}.
\end{aligned}$$

Solving (23) for $\delta p$, $\delta q$ and $\delta z$, we obtain the updating scheme

$$\begin{aligned}
\delta p &= \frac{1}{\Delta}[A_{22}(B_1 + \frac{1}{4}\mu B_3) - A_{12}(B_2 + \frac{1}{4}\mu B_3)] \\
\delta q &= \frac{1}{\Delta}[A_{11}(B_2 + \frac{1}{4}\mu B_3) - A_{12}(B_1 + \frac{1}{4}\mu B_3)] \\
\delta z &= \frac{1}{4}(\delta p + \delta q - B_3)
\end{aligned} \tag{24}$$

where $\Delta = A_{11}A_{22} - A_{12}^2$.

# 7. Results and Conclusions

We tested our adaptive SFS algorithm on synthetic and real images. Due to space limitation, only one synthetic example is presented here. In the experiments, we set $\lambda(x,y) = 1$, $\lambda_{min} = 0.01$, $\mu = 0.1$, $\beta = 1$ and $N_{max}$ for the highest resolution layer be 500. The iterations start from $(p,q,z) = (0,0,0)$. All the images are size of 128x128.

Fig. 1(a) shows the true height map obtained by a laser range finder used to generate the synthetic input image to the algorithm and Fig. 1(b) shows its 3-D plot.

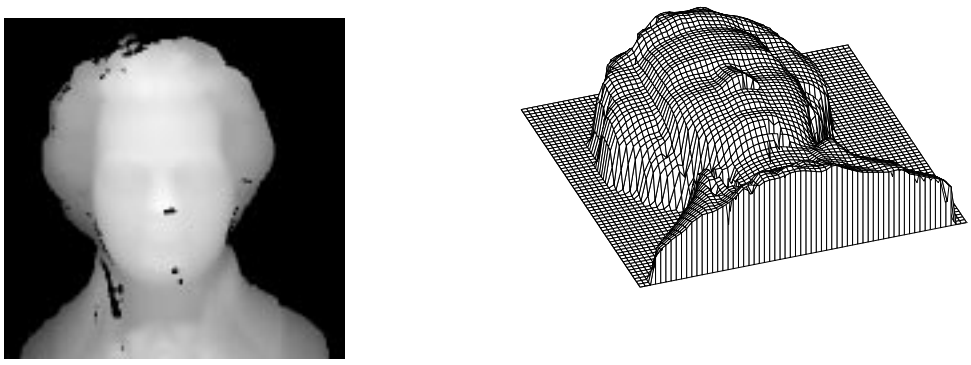

$(a)$ $(b)$

**Figure 1.** Mozart test image: (a) The true height map. (b) A 3-D plot of the true height map.

Fig. 2 shows the synthesized Mozart images with three resolution layers applied to the multiscale iterative scheme. These images are generated from the true height map using Lambertian reflectance map with parameters $\eta = 250$, $\sigma = 45^\circ$ and $\tau = 45^\circ$.

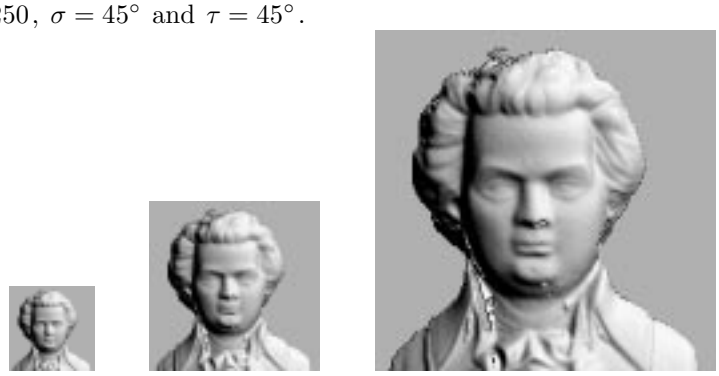

**Figure 2.** The input images, which are synthesized from the true height map with parameters $\eta = 250$, $\sigma = 45^\circ$ and $\tau = 45^\circ$, with sizes 32x32, 64x64 and 128x128 from left to right.

Fig. 3 shows the images with different resolutions synthesized from the $(p, q)$ maps obtained by SFS algorithm using the parameters $\eta = 250$, $\sigma = 45^\circ$ and $\tau = 45^\circ$. The similarity between the input images in Fig. 2 and the reconstructed images in Fig. 3 illustrates that the irradiance requirement is satisfied by the SFS solution.

If we convert our adaptive SFS algorithm to a non-adaptive algorithm by setting a constant value to the regularization parameters, i.e., $\lambda(x, y) = \lambda = 1$, we obtain the three different levels of images shown in Fig. 4 which are synthesized from the $(p, q)$ maps using the reflectance map parameters $\eta = 250$, $\sigma = 45^\circ$ and $\tau = 45^\circ$. If we compare the results shown in Fig. 3 and Fig. 4, we can see that non-adaptive SFS algorithm gives smoother surfaces because of setting a constant value to $\lambda$ which flattens the reconstruction.

**Figure 3.** The images synthesized from the $(p, q)$ maps obtained by the adaptive SFS algorithm using the parameters $\eta = 250$, $\sigma = 45^\circ$ and $\tau = 45^\circ$ with sizes 32x32, 64x64 and 128x128 from left to right.

**Figure 4.** The images synthesized from the $(p, q)$ maps obtained by the non-adaptive SFS algorithm using the parameters $\eta = 250$, $\sigma = 45^\circ$ and $\tau = 45^\circ$ with sizes 32x32, 64x64 and 128x128 from left to right.

The 3-D plots of the reconstructed surfaces obtained by the non-adaptive and adaptive SFS algorithms are given in Fig. 5 with three different resolution levels. The smoothing effect of using a constant $\lambda$ can be easily seen from these plots. It can also be seen that the adaptive control of $\lambda$ improves the solution around discontinuities.

Fig. 6 shows two input images generated with the parameters (a) $\eta = 250$, $\sigma = 45^\circ$, $\tau = 45^\circ$ and (b) $\eta = 250$, $\sigma = 45^\circ$, $\tau = 135^\circ$, and used in photometric stereo as input images.

Fig. 7 shows the images synthesized from the $(p, q)$ maps obtained by integrating the photometric stereo and adaptive SFS algorithm. In Fig. 8, a 3-D plot of the reconstructed height map from this integrated approach is shown. By comparing the results in Fig. 5 and Fig. 8, one can observe that this integration improves the reconstructed surface by providing more symmetrical results with the help of information gathered from two images.

In this paper, an adaptive scheme for recovering shape from shading which reduces smoothing of the reconstructed surface by controlling the smoothness spatially has been developed and implemented. A simple hierarchical implementation of the adaptive SFS algorithm is also presented.

Experimental results show that, the reconstructed surfaces obtained by shape-from-shading method can be improved by adaptively controlling the smoothness parameter, and by combining the photometric stereo and this adaptive SFS method.

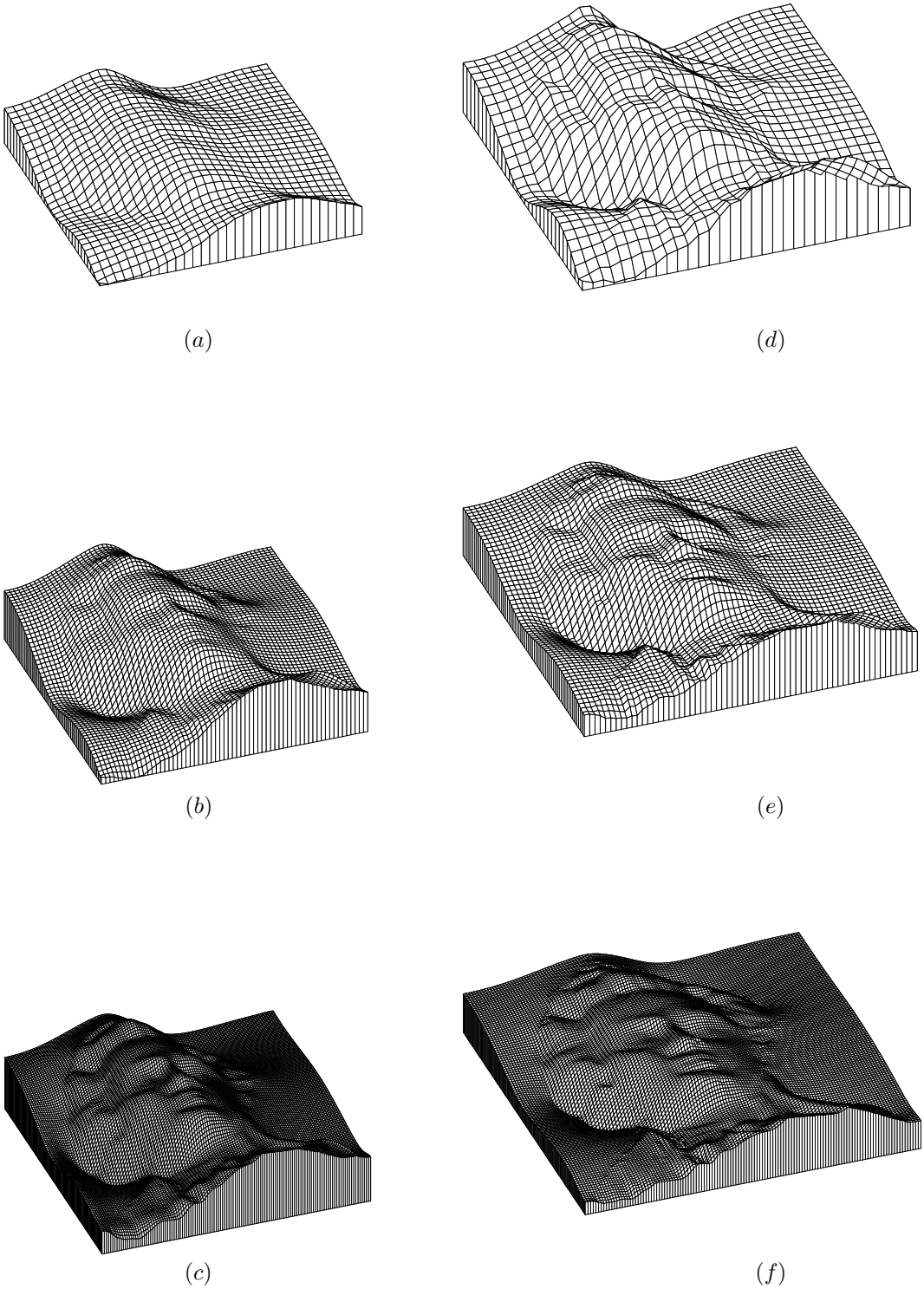


**Figure 5.** The 3-D plots of the reconstructed surfaces obtained by the non-adaptive SFS algorithm with sizes (a) 32x32, (b) 64x64,(c) 128x128 and obtained by the adaptive SFS algorithm with sizes (d) 32x32, (e) 64x64, (f)

128x128.

$(a)$ $(b)$

**Figure 6.** The input images for the adaptive photometric stereo algorithm, which are synthesized from the true height map using the parameters (a) $\eta = 250$, $\sigma = 45^\circ$, $\tau = 45^\circ$ and (b) $\eta = 250$, $\sigma = 45^\circ$, $\tau = 135^\circ$.

$(a)$ $(b)$

**Figure 7.** The images synthesized from the $(p, q)$ maps obtained by the adaptive photometric stereo algorithm using the parameters (a) $\eta = 250$, $\sigma = 45^\circ$, $\tau = 45^\circ$ and (b) $\eta = 250$, $\sigma = 45^\circ$, $\tau = 135^\circ$.

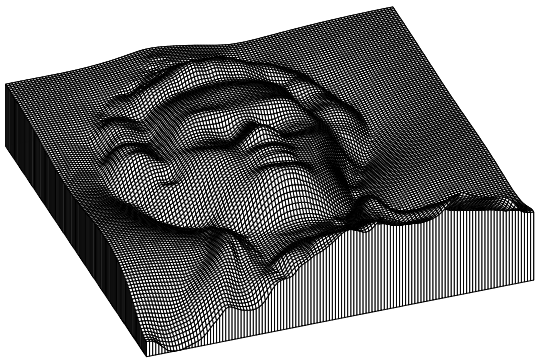

**Figure 8.**A 3-D plot of the reconstructed height map from the adaptive photometric stereo algorithm.

# References

[1] B. K. P. Horn and M. J. Brooks. *Shape from Shading*. The MIT Press, Cambridge, MA, 1989.

[2] B. K. P. Horn. *Shape from Shading: A Method for Obtaining the Shape of a Smooth Opaque Object from One View*. PhD thesis, Department of Electrical Engineering, MIT, 1970.

[3] B. K. P. Horn. Obtaining Shape from Shading Information. In *The Psychology of Computer Vision*, pages 115–155, McGraw-Hill, New York, NY, 1975.

[4] R. J. Woodham. Photometric Method for Determining Surface Orientation from Multiple Images. *Optical Engineering*, 19(1):139–144, January-February 1980.

[5] M. Gökmen and C. C. Li. Edge Detection and Surface Reconstruction using Refined Regularization. *IEEE Trans. on Pattern Analysis Machine Intelligence*, 15(5):492–499, 1993.

[6] B. K. P. Horn. Height and Gradient from Shading. *International Journal of Computer Vision*, pages 37–75, 1990.

[7] B. K. P. Horn and M. J. Brooks. The Variational Approach to Shape from Shading. *Computer Vision, Graphics and Image Processing*, 33(2):174–208, February 1986.

[8] Q. Zheng and R. Chellappa. A Robust Algorithm for Inferring Shape from Shading. Tech. Report, USC-SIPI Rep. 159, Univ. of Southern California, Los Angeles, 1990.

[9] K. Ikeuchi and B. K. P. Horn. Numerical Shape from Shading and Occluding Boundaries. *Artifical Intelligence*, 17(1-3):141–184, August 1981.

[10] Q. Zheng and R. Chellappa. Estimation of Illuminant Direction, Albedo and Shape from Shading. *IEEE Trans. on Pattern Analysis Machine Intelligence*, 13(7):680-702, July 1991.